



Development of a novel method to measure bone marrow fat fraction in older women using high-resolution peripheral quantitative computed

Downloaded from: <https://research.chalmers.se>, 2026-04-05 18:00 UTC

Citation for the original published paper (version of record):

Flehr, A., Källgård, J., Alvé, J. et al (2022). Development of a novel method to measure bone marrow fat fraction in older women using high-resolution peripheral quantitative computed tomography. *Osteoporosis International*, 33(7): 1545-1556. <http://dx.doi.org/10.1007/s00198-021-06224-7>

N.B. When citing this work, cite the original published paper.



Development of a novel method to measure bone marrow fat fraction in older women using high-resolution peripheral quantitative computed tomography

Alison Flehr¹ · Julius Källgård² · Jennifer Alvé^{3,4} · Kerstin Lagerstrand^{5,6} · Evin Papalini^{2,5} · Michael Wheeler¹ · Liesbeth Vandenput^{1,2} · Fredrik Kahl⁷ · Kristian F. Axelsson^{2,8} · Daniel Sundh² · Raghunath Shirish Mysore² · Mattias Lorentzon^{1,2,9} 

Received: 16 April 2021 / Accepted: 26 October 2021
© The Author(s) 2021

Abstract

Summary Bone marrow adipose tissue (BMAT) has been implicated in a number of conditions associated with bone deterioration and osteoporosis. Several studies have found an inverse relationship between BMAT and bone mineral density (BMD), and higher levels of BMAT in those with prevalent fracture. Magnetic resonance imaging (MRI) is the gold standard for measuring BMAT, but its use is limited by high costs and low availability. We hypothesized that BMAT could also be accurately quantified using high-resolution peripheral quantitative computed tomography (HR-pQCT).

Methods In the present study, a novel method to quantify the tibia bone marrow fat fraction, defined by MRI, using HR-pQCT was developed. In total, 38 postmenopausal women (mean [standard deviation] age 75.9 [3.1] years) were included and measured at the same site at the distal ($n=38$) and ultradistal ($n=18$) tibia using both MRI and HR-pQCT. To adjust for partial volume effects, the HR-pQCT images underwent 0 to 10 layers of voxel peeling to remove voxels adjacent to the bone. Linear regression equations were then tested for different degrees of voxel peeling, using the MRI-derived fat fractions as the dependent variable and the HR-pQCT-derived radiodensity as the independent variables.

Results The most optimal HR-pQCT derived model, which applied a minimum of 4 layers of peeled voxel and with more than 1% remaining marrow volume, was able to explain 76% of the variation in the ultradistal tibia bone marrow fat fraction, measured with MRI ($p < 0.001$).

Conclusion The novel HR-pQCT method, developed to estimate BMAT, was able to explain a substantial part of the variation in the bone marrow fat fraction and can be used in future studies investigating the role of BMAT in osteoporosis and fracture prediction.

Keywords Bone marrow adipose tissue (BMAT) · Bone mineral density (BMD) · High-resolution peripheral quantitative computed tomography (HR-pQCT) · Magnetic resonance imaging (MRI)

✉ Mattias Lorentzon
mattias.lorentzon@medic.gu.se

¹ Mary McKillop Institute for Health Research, Australian Catholic University, Melbourne, Australia

² Sahlgrenska Osteoporosis Centre, Institute of Medicine, Sahlgrenska Academy, University of Gothenburg, Gothenburg, Sweden

³ Dept. of Molecular and Clinical Medicine, Inst. of Medicine, Sahlgrenska Academy, University of Gothenburg, Gothenburg, Sweden

⁴ Computer Vision and Medical Image Analysis, Dept. of Electrical Engineering, Chalmers University of Technology, Gothenburg, Sweden

⁵ Medical Physics and Biomedical Engineering, Sahlgrenska University Hospital, Gothenburg, Sweden

⁶ Department of Radiation Physics, Institution of Clinical Sciences, Sahlgrenska Academy, University of Gothenburg, Gothenburg, Sweden

⁷ Department of Electrical Engineering, Chalmers University of Technology, Gothenburg, Sweden

⁸ Region Västra Götaland, Primary Care, Skövde, Sweden

⁹ Region Västra Götaland, Geriatric Medicine, Sahlgrenska University Hospital, Mölndal, Sweden

Introduction

Bone is comprised of an outer dense layer of cortical bone that surrounds a central bone marrow cavity traversed by porous trabecular bone. Bone marrow is primarily composed of red and yellow bone marrow. The red marrow contains hematopoietic cells, that give rise to erythrocytes, and leukocytes as well as mesenchymal stem cells that differentiate into cartilage, bone, or fat. The yellow marrow consists of BMAT, including fat depots of mesenchymal stem cells that have differentiated into marrow adipocytes [1]. BMAT formation begins before birth in the distal skeleton and then later extends throughout the entire bone marrow cavity, such that adults have about 1.6 ± 0.6 L of bone marrow with a 70% average fat fraction [2]. Much of the previous research into bone marrow has focused on the systems and functions of the red marrow [3], as the yellow marrow was considered an inactive ectopic fat reserve [4]. However, more recently, the complex nature of BMAT functioning has begun to emerge.

BMAT has been linked to bone deterioration via several mechanisms. Firstly, it has recently been discovered that similar to visceral and subcutaneous adipose tissues [5], but to a lesser extent, BMAT secretes adipokines (adiponectin and leptin, fatty acids such as palmitate, receptor activator of nuclear factor kappa B ligand [RANKL] and pro-inflammatory cytokines such as TNF- α and IL-6), all of which have the potential to negatively impact bone metabolism [6, 7]. Secondly, marrow adipocytes and osteoblasts are both differentiated from the mesenchymal stem cells, however, aging and estrogen deficiency have both been shown to cause a shift in differentiation by enhancing adipogenesis at the cost of osteoblastogenesis [8, 9]. This loss of the bone-forming osteoblasts decreases bone formation, which increases bone fragility.

As a result, BMAT has been implicated in a number of conditions associated with bone deterioration. Previous studies have associated increased BMAT with osteoporosis [6], anorexia nervosa [10], and diabetes mellitus type II [11]. Numerous studies have also shown an inverse relationship between BMAT and bone mineral density (BMD) [12]. Given the growing evidence of the ubiquitous nature of BMAT, there is increased interest in noninvasive techniques to accurately quantify BMAT. Currently, there are a number of noninvasive magnetic resonance-based imaging (MRI) or computed tomography (CT) based methods available to quantify BMAT [4]. Although MRI is the gold standard for quantifying the fat fraction of the marrow cavity [13], MRI scanners are expensive to use and in high clinical demand which makes them difficult to use in research studies especially large-scale studies. Different quantitative computed tomography (QCT) methods

have also been used to assess BMAT. Dual-energy QCT assessments of vertebral BMAT have shown good agreements with MRI and histologic validations; however, they expose the subject to a relatively high dose of radiation [14]. In recent years, the development of algorithms that allow for the opportunistic screening of conditions such as osteoporosis [15] and vertebral fragility fracture risk [16], for example, from QCT scans obtained via other clinical investigations, have been proposed. However, algorithms that estimate BMAT from such scans have yet to be developed. Therefore, the development of BMAT estimation algorithms using the alternative technique of HR-pQCT, with its low-cost and low-radiation dose performance, is perhaps the more promising for large-scale studies and for use as a potential clinical tool.

The aim of the study was to develop a new method to estimate bone marrow fat using HR-pQCT and to validate the method using MRI fat fraction estimates at the same sites in older women.

Methods

In this study, to develop a method to estimate bone marrow fat using high-resolution peripheral quantitative computed tomography (HR-pQCT), HR-pQCT radiodensity levels at two sites of the distal tibia were compared against MRI fat fraction estimates at the same sites. Both the MRI and HR-pQCT scanning were completed on the same day on all study subjects.

Participants

Women living in Gothenburg and Mölndal were randomly selected from the Swedish population register and mailed invitation packs, inviting them to take part in this calibration study. The exclusion criteria included: living in special housing, unable to walk with or without assistance, unable to communicate in Swedish, history of bilateral hip replacement, history of bilateral lower leg fracture, and unable to undergo an MRI (including use of prosthetic or unable to remain still for 30 min). In total, 168 women were invited and of these, 42 (25%) agreed to participate. The inclusion of the participants was performed in two stages. The first group (S1, $n=22$) was included during 2018 and the second group (S2, $n=20$) was included during 2019. Of the 42 participants, one woman did not proceed with scanning and three participants were excluded due to technical issues, resulting in 38 women in the final analysis.

Ethics approval for the present study was provided by the Regional Ethical Review Board in Gothenburg (registration number 929–12 and 868–16). All procedures were in accordance with the ethical standards and with the Helsinki

Declaration of 1975, as revised in 2000. Written informed consent was obtained from all participants included in the study.

Demographics

Participants' age, height (cm), and weight (kg) were collected using a questionnaire and through standardized measurements. Based on this data, the body mass index (BMI) was calculated as $BMI = [kg/m^2]$.

High-resolution peripheral quantitative computed tomography (HR-pQCT)

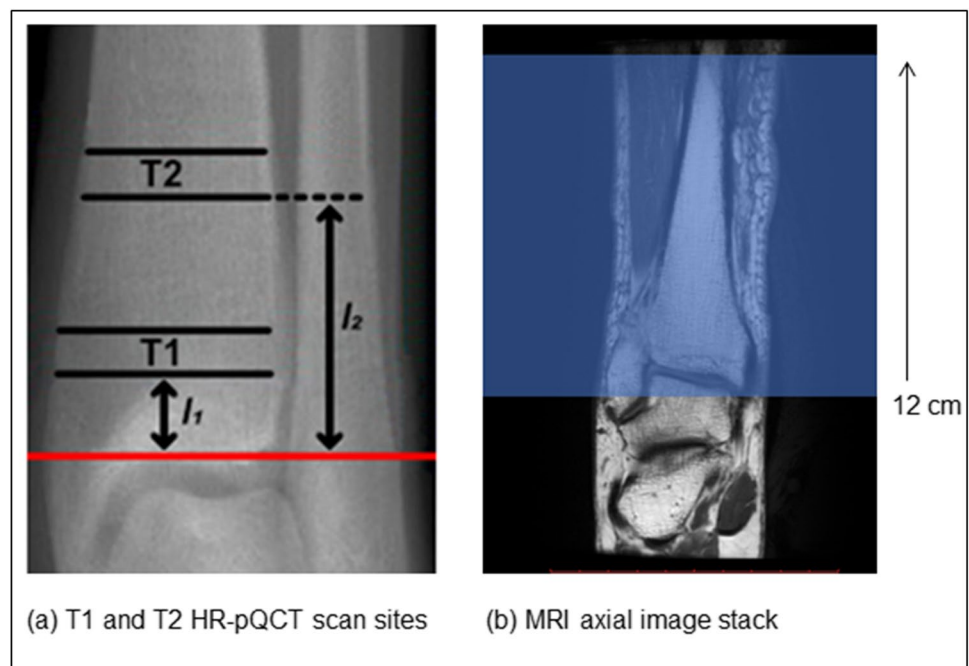
All participants were measured using an HR-pQCT-scanner (XtremeCT, Scanco Medical AG, Brüttisellen, Switzerland). Scanning was performed at two sites on the leg, ipsilateral to the nondominant arm, and if weakness or fracture affecting the selected leg was suspected, the opposite leg was scanned. Each scan consisted of 110 images with a voxel size of $82 \times 82 \times 82 \mu m^3$, covering a region length of 9.02 mm. A reference line was manually placed at the distal tibia joint (Fig. 1a), and the first scan site, the ultradistal site (T1), started 22.5 mm proximal to the reference line at the distal tibia joint. The second scan site, the distal site (T2), represented the distance from the reference line equal to 14% of the total tibia length [17]. Both scans moved in the proximal direction. The ultradistal tibia site was chosen rather than the ultradistal radius site as the tibia is a larger bone than the radius and has a larger bone marrow volume, which aides in the voxel peeling process (allows more voxels to be peeled

and more likely to have a sufficiently large volume for the evaluation of BMAT). Also, the ultradistal radius site has been shown to be more prone to motion artifacts with previous HR-pQCT studies reporting having to exclude 12 and 22%, of images, compared with 3 and 5% of the respective (distal) tibia images [18, 19]. The outer borders of cortical bone were defined by the HR-pQCT software by placing contours adjacent to the periosteum which were manually checked and corrected if needed [18]. Using these contours, a threshold-based method separated cortical from trabecular bone and generated information about the bone geometry and microstructure, such as total volumetric BMD (vBMD; mg/cm^3), cortical vBMD (mg/cm^3), cortical area (mm^2), periosteal circumference (mm), cortical thickness (mm), trabecular volume fraction (%), trabecular number (mm^{-1}), trabecular thickness (mm), and trabecular separation (mm). CVs ranged between 0.2–2.6% for these parameters [18].

Fat-water MRI scanning

Magnetic resonance imaging was performed with a 3T scanner (Discovery MR750w; GE Healthcare, Milwaukee, WI, USA) using the GEM Flex Medium receiver coil. The tibia bone was measured using a 3D multislice, multi-gradient-echo IDEAL IQ sequence: repetition time [TR] = 16.7 ms; first echo time [TE] = 1; Delta TE = 0.8 ms; number of echoes = 6; field of view [FOV] = $180 \times 180 \times 108 mm^3$; flip angle = 3° ; voxel size = $1 \times 1 \times 3 mm^3$; slice thickness = 3 mm; number of slices = 40; no slice gap; pixel bandwidth = 976.5 Hz; number of signal averages = 1. The axial image was planned on a scout scan orthogonally aligned to

Fig. 1 Illustrations of the sites of measurements performed on the right ankle, using either HR-pQCT (a) or MRI (b). For the HR-pQCT, the ultradistal scan site (T1) was 22.5 mm (I_1) from a manually placed reference line (red). The distal scan site (T2) represented the distance from the joint (red line) that was 14% (I_2) of the total tibia length. Each scan covered a region length of 9.02 mm. For the MRI, the axial image stack started at the fibular notch and moved 12 cm in the proximal direction



the tibia. The image stack started at the fibular notch and covered 12 cm (Fig. 1b). Automated linear shimming was performed for each image stack. Participants spent a total time of 20 to 25 min in the MRI scanner, including positioning, scan planning, and scout scanning.

Fat–water MRI processing

An in-house software (AW volume Share 5, GE Advantage Workstation, GE Healthcare, Milwaukee, WI, USA) was used to generate water, fat, $R2^*$, and fat fraction images from the multi-gradient-echo IDEAL IQ scan data. Using a method first described by Dixon [13], the water and fat images were separated from the in-phase and out-of-phase echo signals using iterative decomposition with echo asymmetric and nonlinear least-squares fitting [20–22]. The $R2^*$ images were calculated using mono-exponential fitting of the multiple echo signals. Finally, fat fraction images were determined to quantify the bone marrow fat content and were calculated pixel by pixel from the fat and water images as fat signal/(water signal + fat signal) (Supplement, Figure S1).

MRI and HR-pQCT raw data

All images that were obtained from the MRI and HR-pQCT scans were exported as Digital Imaging and Communications in Medicine (DICOM) folders converted to NIFTI format. Specifically, these raw data files were separated into four sets, containing the two different HR-pQCT scan sites (T1 and T2, Supplement, Figure S2a and S2b, respectively), and two of the six image types obtained from the MRI scanning, i.e., the fat fraction and in-phase images (Supplement, Figure S2c and S2d, respectively).

Extraction of the ROI from MRI images

The region of interest (ROI) containing the bone marrow and the cortical bone were extracted from MRI raw images using MATLAB (MathWorks, Natick, MA, USA). ROI were visually and manually determined by placing rectangular operators around the bone marrow and the cortical bone on each slice individually. By the use of a rectangular operator on each slice of the MRI raw images, a volume of interest containing only the cortical bone and bone marrow was obtained, which was used for the process of registration between HR-pQCT and MRI images.

Registration of the MRI and HR-pQCT images

To register the MRI fat fraction images with the HR-pQCT images and allow a one-to-one voxel relationship for all voxels present in the registered volumes, the online

software ImageJ (Rasband, W.S., NIH, Bethesda, MD, USA), as well as MATLAB (MathWorks, Natick, MA, USA) was used.

Multimodal registration was performed, involving aligning the in-phase MRI volume with the HR-pQCT volume while keeping the HR-pQCT volume fixed in space. The in-phase MRI volume was moved along the fixed HR-pQCT volume until volumetric similarities were matched at the defined scan sites, T1 and T2.

The in-phase MRI images were used in the volumetric alignment procedure as they allowed higher contrast than the fat fraction images. The registration using in-phase MRI images generated a transformation function/matrix which was used for the registration between the Fatfrac MRI images and the HR-pQCT images as both Fatfrac images and the in-phase MRI images had been obtained in the same image space. Figure S3 (Supplement) shows the MRI in-phase images and the corresponding HR-pQCT images at the T1 and T2 sites.

Specifically, the registration transformation was first obtained for MRI in-phase images using the *imregtform* MATLAB function. With the *Imwarp* MATLAB function, the in-phase registration transformation matrix was then used to register the MRI fat fraction volume and the HR-pQCT volume.

Due to the lower spatial resolution of the MRI images [$0:7031 \times 0:7031 \times 3$ mm] compared to the HR-pQCT images [$0:0820 \times 0:0820 \times 0:0820$ mm], each set of 110 HR-pQCT images (T1 and T2) only corresponded to 3 MRI images. To have better accuracy of the registrations and also so that none of the desired slices were excluded during registration, an excess of 1–3 MRI slices were included for the process of registration with HR-pQCT images.

Extraction of the bone marrow volume in the MRI images and assessment of mean fat fraction

Once the MRI fat fraction volume had been registered to the HR-pQCT volume, pixels including undesired regions such as trabeculae and their neighboring pixels were subtracted from the bone marrow volume. Here, subtraction refers to the removal of undesired regions in the volume of interest. Specifically, a mask was created for the HR-pQCT volume which was obtained after registration using the following MATLAB and ImageJ methods: mean, moment, and Otsu's for boundary detection and filling holes (Supplement, Figure S3c and S3d). Only the largest continuous region in the mask defined the final bone marrow volume and was used for data extraction (Supplement, Figure S3e). Then, the mean fat fraction of the bone marrow was calculated from all pixels within the volume.

Assessment of HR-pQCT bone marrow radiodensity

HR-pQCT radiodensity values of the bone marrow were extracted using software developed in MATLAB (MathWorks, Natick, MA, USA) exclusively for this project. With the in-house developed software, the radiodensity was determined pixel by pixel as well as the mean value for the entire scanned volume.

Marrow was defined as all volume inside the cortical bone defined as void of bone. The partial-volume effect can severely affect the radiodensity estimation as bone and marrow attenuate x-rays differently and generate a range of radiodensity values, from + 2000 HU to – 80 HU [19]. Consequently, voxels including both bone and marrow display averages of these differently attenuated tissues (Supplement, Figure S4). In the distal tibia, the bone marrow is traversed by a large number of trabeculae. Therefore, voxels adjacent to trabecular bone can contain spillover from the high attenuating trabeculae with less attenuating marrow, which results in increased radiodensity values. Our developed software read the radiodensity values in all marrow-voxels and calculated means for each scan. To correct for partial-volume effects, voxels adjacent to bone were excluded before calculating the mean radiodensity (Supplement, Figure S4), then the software performed voxel peeling: an optional number of 0 to 10 layers of voxels adjacent to bone were excluded before calculating mean radiodensity (Ind_Vox).

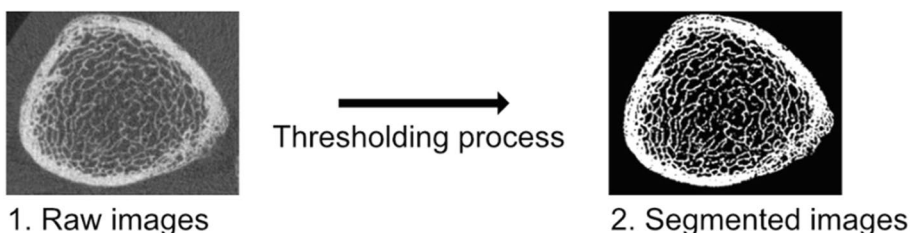
Voxel peeling

To understand how the HR-pQCT intensity values of the bone marrow contributed to the bone marrow fat, voxel peeling of the raw HR-pQCT data was performed. Here, voxel peeling refers to the removal of voxels in the HR-pQCT volume of interest that do not contribute to the MRI-derived fat fraction values, for example, voxels that represent the trabeculae present in the marrow enclosed by cortical bone. The voxel peeling was performed on every voxel including trabeculae as well as immediate neighboring voxels to correct the partial volume effects obtained from the trabeculae. The trabecular bone was identified using the scanner segmented binary HR-pQCT images (Supplement, Figure S5a and S5b), followed by secondary image subtraction. These segmented binary images underwent morphological dilation by a disk-shaped operator, sized depending on the number of voxels that needed to be peeled/removed around the trabeculae, as well as morphological operations such as opening, closing, erosion, and dilation so that the total volume of interest remained the same before and after voxel peeling (Supplement, Figure S6). Figure 2 illustrates the image processing, voxel peeling, and the resulting marrow volume for the HR-pQCT image used for radiodensity analysis.

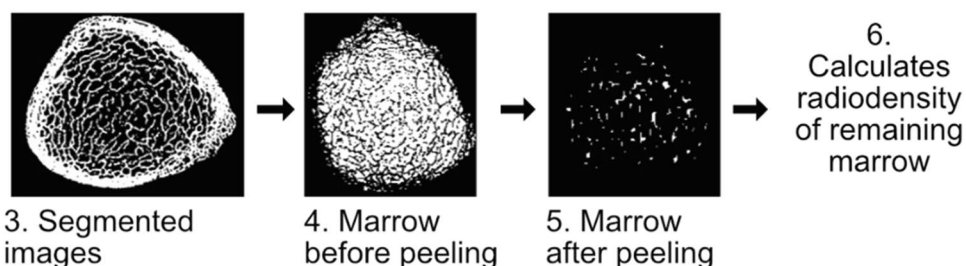
For each scan and number of voxels peeled, the mean radiodensity of all marrow voxels and trimmed means were calculated. Here voxels in the lowest and highest 40% of the distribution of radiodensity were excluded, i.e., voxels in the 40–60% of the distribution remained, the total volume of the marrow before voxel peeling (total volume),

Fig. 2 Assessment of bone marrow fat fraction. **A** Image processing with HR-pQCT standard software. **B** MATLAB analysis. Peeling refers to exclusion of voxels adjacent to bone. Image 5 had 5 layers of voxels peeled

A) HR-pQCT-company software



B) Our software



and remaining bone marrow volume after peeling (volume used) can be seen in Figure S7 (Supplement).

Agreement between MRI and HR-pQCT derived bone marrow fat fraction

Using the linear regression equation ($\beta = -0.031598$ and constant 94.827) for the relationship between Ind_Vox and the MRI-derived fat fraction for the T1 site, predicted fat fraction values were calculated using the Ind_Vox variable. The agreement between the predicted fat fraction values (based on Ind_Vox) and the MRI-derived fat fraction at the T1 level was investigated using a Bland–Altman plot [20]. The limits of agreement were calculated by multiplying the standard deviation of the mean difference between results obtained from the two methods with 1.96.

Statistical methods

Linear regressions analyses of the association between MRI-derived fat fraction and HR-pQCT derived radiodensity were performed (R^2 and p -values are presented) for different voxel peeling alternatives. The two scan sites (T1 and T2) were analyzed separately. Differences between the two study groups were investigated using independent samples t -test. Results are presented as mean value \pm standard deviation (SD) or as median \pm interquartile range (IQR). Associations between MRI-derived fat fractions and HR-pQCT bone parameters were investigated using Pearson bivariate correlations (correlation coefficients r are presented). Assuming a correlation (r) between BMAT methods of at least 0.69, an alpha of 0.05, a minimum of 18 individuals were required to achieve at least 90% statistical power in the analyses. Statistical analyses were performed using SPSS version 26 (IBM, Armonk, NY, USA).

Table 1 Cohort characteristics, MRI derived fat fraction, and HRpQCT bone measurements of the tibia

	Sample 1 ($n = 20$)	Sample 2 ($n = 18$)	Total ($N = 38$)
Age, years, mean (SD)	78.7 (0.7)	72.8 (1.0)	75.9 (3.1)
Height, cm, mean (SD)	161.8 (6.3)	161.4 (5.9)	161.6 (6.0)
Weight, kg, median (\pm IQR)	70.0 (53.5 - 70.0)	61.9 (58.5 - 71.4)	66.2 (58.4 - 73.5)
BMI, kg/m ² , mean (SD)	24.7 (3.5)	25.6 (4.5)	25.2 (4.0)
MRI Bone Marrow fat fraction, %			
Tibia T1, mean (SD)	na	97.9 (1.1)	na
Tibia T2, mean (SD)	97.9 (4.1)	97.7 (1.4)	97.8 (3.11)
HR-pQCT			
Tibia T1 section, mean (SD)			
Total volumetric bone mineral density (mg/cm ³)	na	250.97 (45.79)	na
Cortical area (mm ²)	na	86.52 (24.74)	na
Trabecular area (mm ²)	na	568.46 (128.85)	na
Cortical volumetric bone mineral density (mg/cm ³)	na	759.62 (71.58)	na
Cortical thickness (mm)	na	0.87 (0.27)	na
Periosteal circumference (mm)	na	101.14 (8.95)	na
Trabecular bone volume fraction (%)	na	0.13 (0.04)	na
Trabecular number (mm ⁻¹)	na	1.75 (0.41)	na
Trabecular thickness (mm)	na	0.07 (0.01)	na
Trabecular separation (mm)	na	0.56 (0.32)	na
Tibia T2 section, mean (SD)			
Total volumetric bone mineral density (mg/cm ³)	414.38 (70.29)	437.96 (58.67)	425.55 (65.28)
Cortical area (mm ²)	na	na	157.04 (22.91)
Trabecular area (mm ²)	na	na	260.18 (63.66)
Cortical volumetric bone mineral density (mg/cm ³)	921.31 (37.93)	931.11 (43.17)	925.95 (40.25)
Cortical thickness (mm)	1.94 (0.28)	2.00 (0.24)	1.97 (0.26)
Periosteal circumference (mm)	81.82 (5.93)	78.03 (6.71)	80.02 (6.51)
Trabecular bone volume fraction (%)	0.09 (0.03)	0.09 (0.03)	0.09 (0.03)
Trabecular number (mm ⁻¹)	1.46 (0.41)	1.48 (0.43)	1.47 (0.41)
Trabecular thickness (mm)	0.06 (0.02)	0.06 (0.02)	0.06 (0.02)
Trabecular separation (mm)	0.67 (0.18)	0.72 (0.46)	0.69 (0.34)

Results

Cohort characteristics

Cohort characteristics, including anthropometrics, MRI-derived bone marrow fat fraction, and HR-pQCT bone variables of the tibia are presented for the whole cohort in Table 1. Women included in the present study were, on average, 75.9 years old, 161.1 cm tall, had a median weight of 66.2 kg, and an average BMI of 25.2 (Table 1). Using independent sample *t*-tests, the women in samples 1 and 2 were not found to differ significantly in height, weight or BMI, and MRI-derived fat fractions. However, the women in sample 1 were significantly older than the women in sample 2 ($p < 0.001$).

Evaluating the optimal number of voxel peels

At the ultradistal tibial section (Table 2), the best HR-pQCT-derived radiodensity predictor of MRI-derived fat fractions (highest R^2 value) was observed using 5 layers of voxel peels, explaining 69.9% ($R^2 = 0.699$) of the variation in the MRI-derived bone marrow fat fraction, based on a remaining median volume used (remaining bone marrow) of 1.1%. At the distal tibial section (Supplement, Table S1), the optimal HR-pQCT-derived radiodensity predictor of MRI-derived fat fractions was observed for 7 layers of voxel peels, which could explain 19.1% of the variation in the MRI-derived bone marrow fat fraction ($R^2 = 0.191$), utilizing a median remaining volume of 2.5%.

The percent of the variation of the MRI-derived marrow fat fraction explained by HR-pQCT-derived radiodensity values decreased as the number of individuals with small percentages of bone marrow volume remaining (i.e., $< 0.1\%$ volume used) increased, also the predictive power of the HR-pQCT-derived radiodensity values decreased substantially (Table 2 and Table S1). Lastly, the mean and median values of “volume used” at both scan sites appeared to be asymmetrically distributed and diverged increasingly with number of voxels peeled.

There was a substantial variation in the remaining bone marrow (volume used) and trabecular bone structure between individuals at both scan sites. For example, after 5 layers of voxel peeling, the range in “volume used” was 0.01 to 36% for the T1 scan site and 0.4 to 65% for the T2 scan site. There were large variations in trabecular bone microstructure found within the S2 cohort (Supplement, Figure S8). T1 segmented HR-pQCT images from 3 cases before voxel peeling, were ranked from 1 to 18 by their remaining volume of bone marrow (volume used) after 5 layers of voxel peeling and displayed large differences in remaining volume used (from $< 1\%$ to over 35%).

Overall, these results suggest that voxel peeling enhances the accuracy of the fat estimation quantification until the volume of bone marrow voxels falls below a critical threshold and the estimations quantification becomes unreliable. Furthermore, due to a large amount of bone marrow variance between individuals, an algorithm was developed that could be applied at an individual level. That is, for any given case, a maximum number of voxel peels was applied (ranging from 4 to 10) with a remaining bone marrow volume used

Table 2 Associations between fat fractions measured by MRI and HR-pQCT-derived radiodensity levels at the ultradistal tibia site (T1)

Number of voxel peels	R^2 (S2 ¹) ($n = 18$)	Mean volume used (%)	Median volume used (%)	Number of individuals $< 1\%$ volume used	Number of individuals $< 0.1\%$ volume used	Number of individuals missing volume	Mean radiodensity (HU)
0	0.334	100	100	0	0	0	193
1	0.461	60	59	0	0	0	2.3
2	0.538	30	28	0	0	0	-44
3	0.637	14	11	0	0	0	-63
4	0.681	6.6	3.8	1	0	0	-84
5	0.699	3.6	1.1	8	1	0	-98
6	0.644	2.4	0.28	14	4	0	-103
7	0.368	1.8	0.070	16	11	0	-103
8	0.379	1.6	0.012	16	14	1	-111
9	0.171	1.4	0.0024	16	13	3	-114
10	0.133	1.2	0.0002	17	16	7	-70

Linear regression derived R^2 values for fat fractions, measured using MRI, predicted by HR-pQCT-derived radiodensity values for voxel peel layers 1 to 10 at the T1 scan site (sample group 2 [$n = 18$]). For each voxel peel the of mean and median volume used (remaining volume of bone marrow), the number of individuals with $< 1\%$ and $< 0.1\%$ volume used, and Hounsfield units (HU) were also calculated. 1. Only data from sample group 2 (S2) was available from the scanning at the T1 site

HU: Hounsfield units

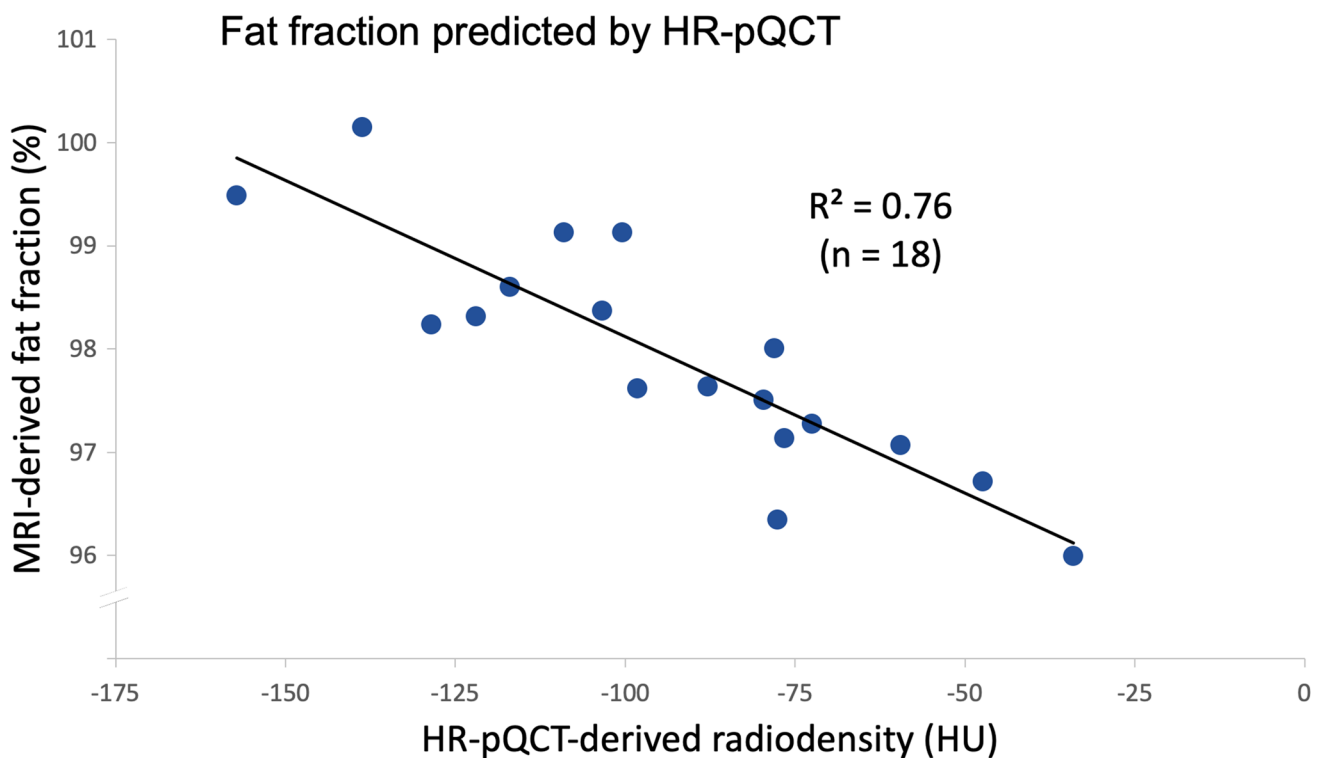


Fig. 3 Association between MRI-derived fat fraction and HR-pQCT-derived radiodensity values at the T1 scan site investigated using linear regression. Radiodensity was obtained by individual voxel peel-

ing and required >1% volume used (Ind_Vox). Abbreviations: HU: Hounsfield units; MRI: magnetic resonance imaging; HR-pQCT: high-resolution peripheral quantitative computed tomography

greater than 1%. This procedure was found to enhance the prediction of MRI-derived bone marrow fat fraction at the T1 scan site, where individual peeling yielded an $R^2=0.76$ ($p<0.001$; Fig. 3) compared with an $R^2=0.70$ ($p<0.001$) for 5 voxel nonindividual peeling (Table 2). However, individual voxel peeling was not found to enhance fat prediction at the T2 scan site, where the highest individual peel yielded an $R^2=0.12$ ($p<0.05$), compared with the highest R^2 of 0.19 ($p<0.01$) for nonindividual peeling (Supplement, Table S1).

Pearson bivariate correlations (correlation coefficient r) were performed to examine how the HR-pQCT radiodensity parameter (Ind_Vox) with the highest R^2 (Fig. 3) compared with the MRI-derived fat fractions and standard HR-pQCT derived bone parameters at the T1 (Supplement, Table S2) and T2 sites (Supplement, Table S3). At the ultradistal tibia site (T1), the MRI-derived fat fraction was most strongly inversely correlated with Ind_Vox ($r=-0.871$, $p<0.01$), followed by trabecular bone volume fraction ($r=-0.609$; Supplement, Table S2). The MRI-derived marrow fat fraction and at the distal tibia site (T2) was most strongly inversely correlated to Vox7_mean 40–60 ($r=-0.437$, $p<0.01$), followed by trabecular area ($r=0.101$, not significant; Supplement, Table S3).

The agreement between the predicted bone marrow fat fraction (derived from Ind_Vox) and the MRI-derived bone

marrow fat fraction was illustrated using a Bland–Altman plot (Fig. 4). The mean (standard deviation) difference between the predicted (based on Ind_Vox) and actual (MRI) in the bone marrow fat fraction was -0.0001 (0.54)%. In all investigated individuals, the difference in bone marrow fat fraction between methods was within the limits of agreement.

Discussion

In the present study, a novel method to estimate BMAT in the ultradistal tibia using HR-pQCT was developed and validated against state-of-the-art MRI-derived fat fractions. The most optimal HR-pQCT model was able to explain up to 76% of the variation in the MRI-derived fat fraction at the ultradistal tibia. These results suggest that voxel peeling, preferentially on an individual level, based on the available bone void volume in the marrow compartment, can enhance the accuracy of fat fraction quantification and indicate that HR-pQCT scanning at the ultradistal site has the potential to a high degree estimate BMAT quantity in older women.

It has been proposed that BMAT has a role in the pathogenesis of osteoporosis, implying that quantification of BMAT could potentially enhance the diagnosis of

Agreement between MRI and HRpQCT derived bone marrow fat fraction (%)

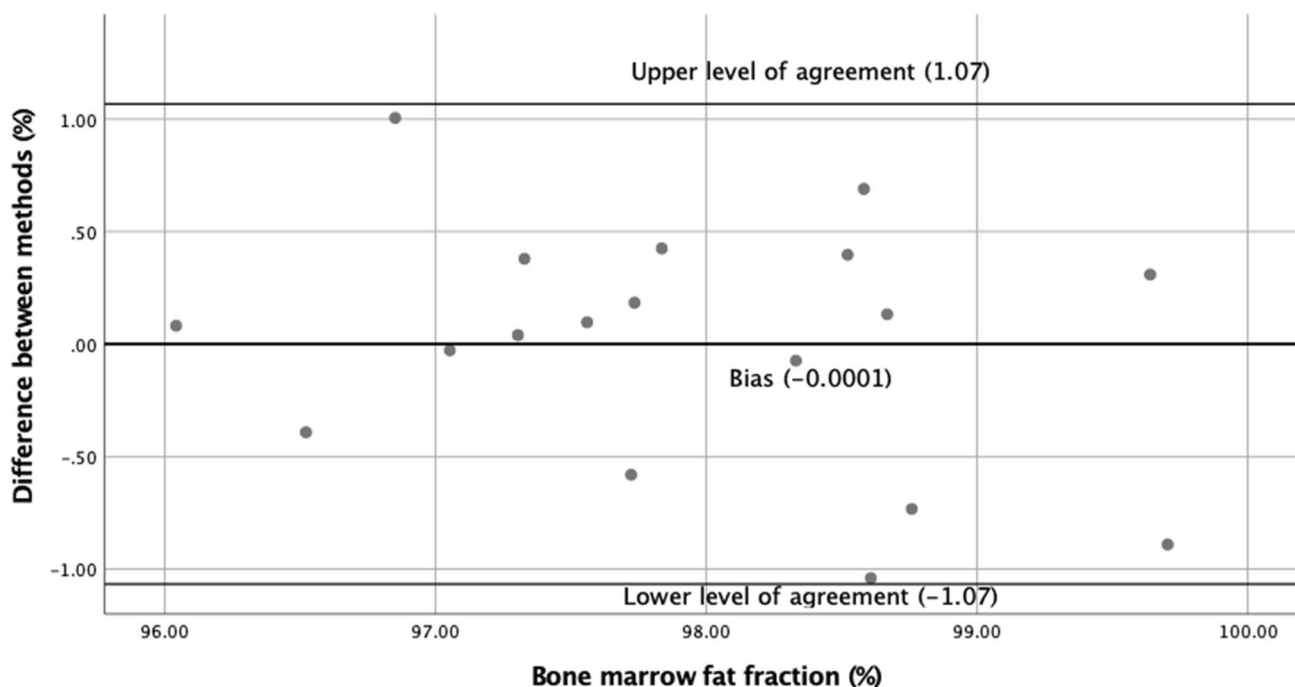


Fig. 4 Agreement between bone marrow fat (%) at the ultradistal site (T1) between the HRp-QCT derived method Ind_Vox and MRI derived bone marrow fat fraction described in a Bland–Altman plot. Upper and lower levels of agreement ($\pm 1.96 \times$ the standard deviation

of the difference between bone marrow fat fraction values from the 2 methods), as well as method bias, are presented. MRI: Magnetic Resonance Imaging; HR-pQCT: High-resolution peripheral quantitative computed tomography

osteoporosis and improve fracture prediction [21]. Osteoporosis is a disease characterized by deteriorated bone microstructure and low BMD, resulting in an increased risk of fracture [22].

Nuclear magnetic resonance includes MRI and MR spectroscopy (MRS), both techniques depend on the hydrogen atom nuclei (consisting of a single proton) which is abundant in the water and fat of the human body [13]. Both techniques are able to quantify adipose tissue but only MRS can measure lipid composition, including saturated and unsaturated lipids [21]. The herein used method Dixon-MRI or chemical shift-encoding-based water-fat MRI has been developed to measure bone marrow fat, by using standardized fat fractions maps. A study on human specimens found that a Dixon imaging and iterative decomposition of fat and water with echo asymmetry and least-squares estimation (IDEAL) reconstruction was highly correlated, with R^2 equal to 97%, to the known marrow fat fraction [23].

Several previous studies have reported an inverse association between MRI or MRS quantified BMAT, BMD measured with DXA, and volumetric BMD of especially the trabecular, but also of the cortical bone, measured using QCT [21, 24–26]. In Icelandic women, but not in men, greater baseline MRS-derived vertebral BMAT was associated with

an increased rate of loss of volumetric BMD at the spine and of trabecular BMD at the femoral neck [27].

Given the association between BMAT and BMD, which is an important determinant of bone strength [28], a relationship between BMAT quantity and fracture risk could be anticipated. Higher vertebral MRS-derived BMAT has been associated with a prevalent vertebral fracture in Icelandic older men and women [29]. However, in another study of fracture patients and controls, there were no differences in BMAT quantity, but lipid saturation levels differed between groups [11]. As of yet, no well-powered studies have investigated if the measurement of BMAT can predict incident fractures.

Although QCT can be used to estimate BMAT as well as cortical and trabecular bone, the low resolution and presence of trabecular bone in the marrow compartment in combination with the partial volume effect, which gives rise to falsely high density in marrow voxels adjacent to bone, limits the usefulness of the technique to estimate BMAT quantity. Our results clearly demonstrate that voxels located close to the bone tissue displayed unrealistically high radiodensity values. Using voxel peeling to remove voxels adjacent to the bone yielded radiodensity values more in the expected range, 0 to –120 Hounsfield units, and improved the correlations

to MRI-derived fat fraction values, supporting the benefit of voxel peeling.

Such limitations would also likely impact the viability of any BMAT estimation algorithms that might be developed and applied to QCT scans opportunistically obtained via other clinical investigations. Furthermore, the relatively high radiation with the associated and expected increase in cancer cases [30] prevents QCT from being a commonly utilized screening or prediction tool in humans. A quick, noninvasive, more cost-efficient procedure to measure BMAT, without a high radiation dose, has several potential applications. A recent HR-QCT study demonstrated that two different methods (one utilizing voxel peeling and one based on morphological filtering) were able to detect bone void marrow space with high accuracy, using HR-pQCT with much higher resolution as the gold standard, allowing the measurement of mineral equivalent marrow density with HRQCT [31]. Here, a densitometric assessment of the bone marrow in vertebral specimens was obtained from an *ex vivo* osteoporotic cohort, and consequently, the used methodologies and outcomes are limited to that investigated clinical population. However, it should be emphasized that HR-pQCT scanning of high resolution and voxel peeling does not eliminate the partial volume effects completely. The much higher bone density will spill over onto bone void voxels. In the herein presented analysis (Figure S7), a considerable proportion of the voxels ranged from 0 to + 1000 Hounsfield units, far from the expected 0 to – 120 Hounsfield units, even though 3 layers of voxels were peeled from the edge of the detected bones prior to analysis of voxel density. Another method utilizing HR-pQCT to identify marrow void space that could serve as a proxy representation of BMAT [32] was recently presented. However, the ability of this method to quantify BMAT has not been tested.

Recently, a novel HR-pQCT based method was used to measure the fraction of adipose tissue over the total volume of the marrow cavity (AV/TV), in order to define a function of the marrow fat proportion and the relative medullary density (MAI). AV/TV was strongly correlated to the adipose tissue area detected using histology in sheep radii and MAI was able to discriminate 77 women with a recent nonvertebral fracture from 226 controls [33]. Although MAI was higher in fracture cases than in controls, the study did not establish if MAI was able to predict incident fractures.

A strength of the present study design was that it included validation of HR-pQCT derived radiodensities of the BMAT using MRI-derived fat fractions. To our knowledge, no prior study has validated the ability to estimate BMAT from HR-pQCT scanning using human MRI fat fraction scanning. Moreover, the novel method with its dedicated software

tool had the advantage that it can be applied retrospectively on studies where subjects have previously undergone HR-pQCT scanning. Further, the dedicated software tool enables correction of partial volume effects by including peeling of voxels adjacent to the bone and thereby excluding unreliable voxels.

The present study had several limitations. First, the number of participants in this study was restricted by insufficient access to the MRI scanner due to its high clinical demand. Also, due to inadequate positioning at MRI scanning, only study group 2 had complete data covering also the T1 scan site. Second, the HR-pQCT technique was designed to measure dense bone tissue and not marrow cavity fat or water, which likely increases the measurement error. Third, the influence of beam-hardening on BMAT radiodensities was not fully explored and, thus, further validation is needed. Fourth, only a small portion of bone marrow was assessed as the length of the cylindrical region covered by each scan was 9 mm, and only ~2% on average of the marrow inside each region was used for the mean BMAT radiodensity calculations. Nonetheless, a high correlation with the MRI-derived fat fraction was still established using this small volume. Fifth, the resolution of the MRI was relatively low and although we used the established IDEAL algorithm, slight inaccuracies in the fat fraction estimates were made obvious by the fact that a few subjects presented mean fat fraction estimates above 100%, with a maximum value of 101.2%. The mean fat fraction estimate was based on all voxels within the cortical bone, including also trabecular bone. However, it seems unlikely that the presence of trabecular bone would have lowered the fat fraction significantly as the mean fat fractions were as high as close to 100%. Sixth, the results of the present study are limited to cohorts similar to that of the study cohort and our developed methodology needs to be validated in further populations before our method can be generalized to the wider population. Seventh, as HR-pQCT is currently used as a research tool, any implementation of a HR-pQCT-based method to assess BMAT in clinical practice would not be possible.

In conclusion, we developed a new and rapid HR-pQCT-based method for quantifying BMAT at ultradistal tibia in older women. This technique could be used on already collected HR-pQCT images in order to evaluate how different interventions or conditions, such as diabetes and anorexia, affect the quantity of BMAT and how it is associated with various outcomes, including incident fractures.

Supplementary Information The online version contains supplementary material available at <https://doi.org/10.1007/s00198-021-06224-7>.

Funding Open access funding provided by University of Gothenburg.

Declarations

Conflict of interest Professor Lorentzon has received lecture and/or consulting fees from Amgen, Astellas, Lilly, Meda, Renapharma, Radius Health, Renapharma, UCB Pharma, Meda, and Consilient Health, Tromp Medical-Hologic, all outside the scope of the submitted work. Dr. Axelsson has received lecture fees from Lilly, Meda/Mylan, and Amgen, all outside the scope of the submitted work. All other authors have no conflicts of interest.

Open Access This article is licensed under a Creative Commons Attribution-NonCommercial 4.0 International License, which permits any non-commercial use, sharing, adaptation, distribution and reproduction in any medium or format, as long as you give appropriate credit to the original author(s) and the source, provide a link to the Creative Commons licence, and indicate if changes were made. The images or other third party material in this article are included in the article's Creative Commons licence, unless indicated otherwise in a credit line to the material. If material is not included in the article's Creative Commons licence and your intended use is not permitted by statutory regulation or exceeds the permitted use, you will need to obtain permission directly from the copyright holder. To view a copy of this licence, visit <http://creativecommons.org/licenses/by-nc/4.0/>.

References

- Schäffler A, Büchler C (2007) Concise review: adipose tissue-derived stromal cells—basic and clinical implications for novel cell-based therapies. *Stem cells* 25:818–827
- Scheller EL, Cawthorn WP, Burr AA, Horowitz MC, Macdougald OA (2016) Marrow adipose tissue: trimming the fat. *Trends Endocrinol Metab* 27:392–403
- Steer K, Stavnichuk M, Morris M, Komarova SV (2017) Bone health in patients with hematopoietic disorders of bone marrow origin: systematic review and meta-analysis. *J Bone Miner Res* 32:731–742
- Bani Hassan E, Ghasem-Zadeh A, Imani M, Kutaiba N, Wright DK, Sephehrizadeh T, Duque G (2019) Bone marrow adipose tissue quantification by imaging. *Curr Osteoporos Rep* 17:416–428
- Fantuzzi G (2005) Adipose tissue, adipokines, and inflammation. *Journal of Allergy and clinical immunology* 115:911–919
- Herrmann M (2019) Marrow fat-secreted factors as biomarkers for osteoporosis. *Curr Osteoporos Rep* 17:429–437
- Li Y, Meng Y, Yu X (2019) The unique metabolic characteristics of bone marrow adipose tissue. *Frontiers in Endocrinol* 8(10):69
- Paccou J, Hardouin P, Cotten A, Penel G, Cortet B (2015) The role of bone marrow fat in skeletal health: usefulness and perspectives for clinicians. *J Clin Endocrinol Metab* 100:3613–3621
- Moerman EJ, Teng K, Lipschitz DA, Lecka-Czernik B (2004) Aging activates adipogenic and suppresses osteogenic programs in mesenchymal marrow stroma/stem cells: the role of PPAR- γ 2 transcription factor and TGF- β /BMP signaling pathways. *Aging Cell* 3:379–389
- Bredella MA, Fazeli PK, Miller KK, Misra M, Torriani M, Thomas BJ, Ghomi RH, Rosen CJ, Klibanski A (2009) Increased bone marrow fat in anorexia nervosa. *J Clin Endocrinol Metab* 94:2129–2136
- Patsch JM, Li X, Baum T, Yap SP, Karampinos DC, Schwartz AV, Link TM (2013) Bone marrow fat composition as a novel imaging biomarker in postmenopausal women with prevalent fragility fractures. *J Bone Miner Res* 28:1721–1728
- Schwartz AV (2015) Marrow fat and bone: review of clinical findings. *Front Endocrinol (Lausanne)* 6:40
- Glover GH (1991) Multipoint Dixon technique for water and fat proton and susceptibility imaging. *J Magn Reson Imaging* 1(5):521–30
- Arentsen L, Yagi M, Takahashi Y, Bolan PJ, White M, Yee D, Hui S (2015) Validation of marrow fat assessment using noninvasive imaging with histologic examination of human bone samples. *Bone* 72:118–122
- Pickhardt PJ, Pooler BD, Lauder T, del Rio AM, Bruce RJ, Binkley N (2013) Opportunistic screening for osteoporosis using abdominal computed tomography scans obtained for other indications. *Ann Intern Med* 158:588–595
- Lee S, Binkley N, Lubner M, Bruce R, Ziemlewicz T, Pickhardt P (2016) Opportunistic screening for osteoporosis using the sagittal reconstruction from routine abdominal CT for combined assessment of vertebral fractures and density. *Osteoporos Int* 27:1131–1136
- Sundh D, Nilsson AG, Nilsson M, Johansson L, Mellstrom D, Lorentzon M (2017) Increased cortical porosity in women with hip fracture. *J Intern Med* 281:496–506
- Larsson B, Mellström D, Johansson L, Nilsson AG, Lorentzon M, Sundh D (2018) Normal bone microstructure and density but worse physical function in older women treated with selective serotonin reuptake inhibitors, a cross-sectional population-based study. *Calcif Tissue Int* 103:278–288
- Nilsson M, Sundh D, Ohlsson C, Karlsson M, Mellström D, Lorentzon M (2014) Exercise during growth and young adulthood is independently associated with cortical bone size and strength in old Swedish men. *J Bone Miner Res* 29:1795–1804
- Bland JM, Altman DG (1986) Statistical methods for assessing agreement between two methods of clinical measurement. *Lancet* 1:307–310
- Li X, Schwartz AV (2020) MRI Assessment of bone marrow composition in osteoporosis. *Curr Osteoporos Rep* 18(1):57–66
- Lorentzon M, Cummings SR (2015) Osteoporosis: the evolution of a diagnosis. *J Intern Med* 277:650–661
- Gee CS, Nguyen JT, Marquez CJ et al (2015) Validation of bone marrow fat quantification in the presence of trabecular bone using MRI. *J Magn Reson Imaging* 42:539–544
- Kim TY, Schwartz AV, Li X et al (2017) Bone marrow fat changes after gastric bypass surgery are associated with loss of bone mass. *J Bone Miner Res* 32:2239–2247
- Baum T, Yap SP, Karampinos DC, Nardo L, Kuo D, Burghardt AJ, Masharani UB, Schwartz AV, Li X, Link TM (2012) Does vertebral bone marrow fat content correlate with abdominal adipose tissue, lumbar spine bone mineral density, and blood biomarkers in women with type 2 diabetes mellitus? *J Magn Reson Imaging* 35:117–124
- Shen W, Chen J, Punyanitya M, Shapses S, Heshka S, Heymsfield SB (2007) MRI-measured bone marrow adipose tissue is inversely related to DXA-measured bone mineral in Caucasian women. *Osteoporos Int* 18:641–647
- Woods GN, Ewing SK, Sigurdsson S et al (2020) Greater bone marrow adiposity predicts bone loss in older women. *J Bone Miner Res* 35:326–332
- Marshall D, Johnell O, Wedel H (1996) Meta-analysis of how well measures of bone mineral density predict occurrence of osteoporotic fractures. *BMJ* 312:1254–1259

29. Schwartz AV, Sigurdsson S, Hue TF et al (2013) Vertebral bone marrow fat associated with lower trabecular BMD and prevalent vertebral fracture in older adults. *J Clin Endocrinol Metab* 98:2294–2300
30. Brenner DJ, Hall EJ (2007) Computed tomography—an increasing source of radiation exposure. *N Engl J Med* 357:2277–2284
31. Peña JA, Thomsen F, Damm T, Campbell GM, Bastgen J, Barkmann R, Glüer CC (2016) Bone-marrow densitometry: assessment of marrow space of human vertebrae by single energy high resolution-quantitative computed tomography. *Med Phys* 43:4174–4183
32. Whittier DE, Burt LA, Boyd SK (2020) A new approach for quantifying localized bone loss by measuring void spaces. *Bone* 143:115785
33. Zebaze R, Osima M, Bui M et al (2019) Adding marrow adiposity and cortical porosity to femoral neck areal bone mineral density improves the discrimination of women with nonvertebral fractures from controls. *J Bone Miner Res* 34(8):1451–1460

Publisher's note Springer Nature remains neutral with regard to jurisdictional claims in published maps and institutional affiliations.